CORONARY ANGIOGRAPHY

Comparison of Radial and Cartesian Imaging Techniques for MR Coronary Angiography

Cosima Jahnke, M.D.,[1,2,*] **Ingo Paetsch,**[1] **Bernhard Schnackenburg,**[1]
Rolf Gebker,[1] **Uwe Köhler,**[1] **Axel Bornstedt,**[1] **Eckart Fleck,**[1]
and Eike Nagel[1]

[1]Department of Internal Medicine/Cardiology, German Heart Institute,
Berlin, Germany
[2]Department of Internal Medicine/Cardiology,
University of Freiburg, Freiburg, Germany

ABSTRACT

Background: Magnetic resonance coronary angiography (MRCA) has traditionally been performed using a Cartesian k-space data acquisition scheme. Radial k-space sampling is known to be less sensitive to motion artifacts. Thus, potential improvements may be achieved with radial k-space data acquisition using steady state free precession (SSFP) techniques. We directly compared SSFP three-dimensional (3D)-MRCA using radial and Cartesian data acquisition. *Methods:* Forty-four consecutive patients with suspected coronary artery disease underwent free-breathing, navigator-corrected MRCA of the left or right coronary artery using SSFP (TR/TE/flip angle: 4.5 ms/2.3 ms/90°) with radial and again with Cartesian k-space filling. Quantitative MRCA was performed with a dedicated multiplanar reformatting software to determine: visual score for image quality (low=1, high=4), vessel sharpness, visible vessel length, number of visible side branches, and average vessel diameter. Diagnostic accuracy for detection of $\geq 50\%$ coronary artery stenosis was calculated in comparison to invasive X-ray angiography. *Results:* Radial data acquisition resulted in a significant ($p < 0.01$) increase in vessel sharpness ($55.6 \pm 7.2\%$ vs. $45.9 \pm 7.0\%$) but a decrease in average vessel diameter (2.6 ± 0.5 mm vs. 3.0 ± 0.4 mm), number of visible side branches (2.1 ± 1.1 vs. 3.0 ± 1.7) and number of assessable coronary artery segments (66% vs. 73%) compared to Cartesian approach. There was no significant difference regarding the diagnostic accuracy (80.8% vs. 83.9%), the visual score (2.6 ± 0.9 vs. 3.0 ± 0.9) and the visible vessel length

Correspondence: Cosima Jahnke, M.D., Internal Medicine/Cardiology, University of Freiburg, Hugstetter Str. 55, Freiburg 79106, Germany; Fax: +49-761-270-3767; E-mail: jahnke@med1.ukl.uni-freiburg.de.

(92.1±36.0 mm vs. 99.9±32.4 mm). *Conclusions:* MRCA with radial k-space sampling appears to be on a par with Cartesian approach with respect to the diagnostic performance in an unselected patient population. Nevertheless, with current implementations, radial sampling is inferior to Cartesian sampling regarding the visualization of side branches despite better vessel sharpness.

Key Words: Magnetic resonance imaging; Magnetic resonance coronary angiography; Coronary disease; Radial data acquisition.

INTRODUCTION

Although coronary magnetic resonance angiography (MRA) evolved rapidly (Kim et al., 2001; Li et al., 1996; Manning et al., 1993b; Pennell et al., 1993), visualization of the whole coronary arterial tree with reproducibly high diagnostic image quality remains challenging. Implementation of flow-independent steady-state free precession (SSFP) techniques yielded high-quality coronary MRA due to the inherently high signal-to-noise ratio and a favourable contrast between the coronary blood and the surrounding tissue (Duerk et al., 1998; Shea et al., 2002). Additionally, SSFP sequences resulted in superior image quality and improved vessel border definition in comparison to conventional T2-prepared gradient-echo imaging (Spuentrup et al., 2002, 2003a). Thus, SSFP sequences are gaining increasing acceptance in coronary artery imaging (Deshpande et al., 2001).

In order to improve reliable depiction of the whole coronary arterial tree, it is of special importance to compensate for extensive vessel movement caused by respiration and cardiac contraction. The adverse impact of breathing-induced myocardial motion can be minimized by breath holding (Li et al., 2001; Manning et al., 1993a; Pennell et al., 1993; Regenfus et al., 2003) or by respiratory gating using the MR navigator technique (Danias et al., 1997; Stuber et al., 1999a); motion artifacts due to cardiac contraction and relaxation can be minimized by shortening the duration of data acquisition per heartbeat and performing data readout during the coronary artery rest period. In our institution, we regard the navigator technique as preferable, facilitating the use of a higher spatial resolution within a three-dimensional (3D) volume as large as desirable. However, many patients have an unfavourable breathing pattern or present with arrhythmia, leading to reduced image quality or prolonged measurement times. In order to shorten scan duration and improve signal-to-noise ratio, more efficient k-space sampling schemes, such as echo planar (Bornert and Jensen, 1995; Botnar et al., 1999a) and spiral imaging (Bornert et al., 2001; Thedens et al., 1999; Yang et al., 2003), have been proposed. Additionally, coronary MRA may be further improved with radial k-space data acquisition, since radial acquisition techniques are less sensitive to motion artifacts (Glover and Pauly, 1992).

Thus, the aim of the present study was to directly compare radial and Cartesian data acquisition techniques for coronary MRA with regard to image quality and diagnostic accuracy.

METHODS

Subjects

Forty-four patients (29 males, 15 females; age 58.1 years, range 31–81 years) were studied. All patients were scheduled for diagnostic coronary angiography due to clinically suspected coronary artery disease. Patients with contraindications to MR imaging (e.g., cardiac pacemakers, other ferromagnetic implants, or claustrophobia) were excluded from the study. Written informed consent was obtained from all patients and the study was approved by the Ethics Committee of the Virchow Klinikum and Charité, Berlin, Germany.

Table 1. Scan characteristics of the 44 patients for Cartesian and radial data acquisition scheme.

	Navigator efficiency (%)	Effective scan duration (s)	Acquisition duration (ms)	Heart rate (1/min)
Cartesian	46.3±16.0	513±187	76.6±5.4	76±24
Radial	49.0±15.5	612±198**	76.5±5.6	76±25

**p<0.01.
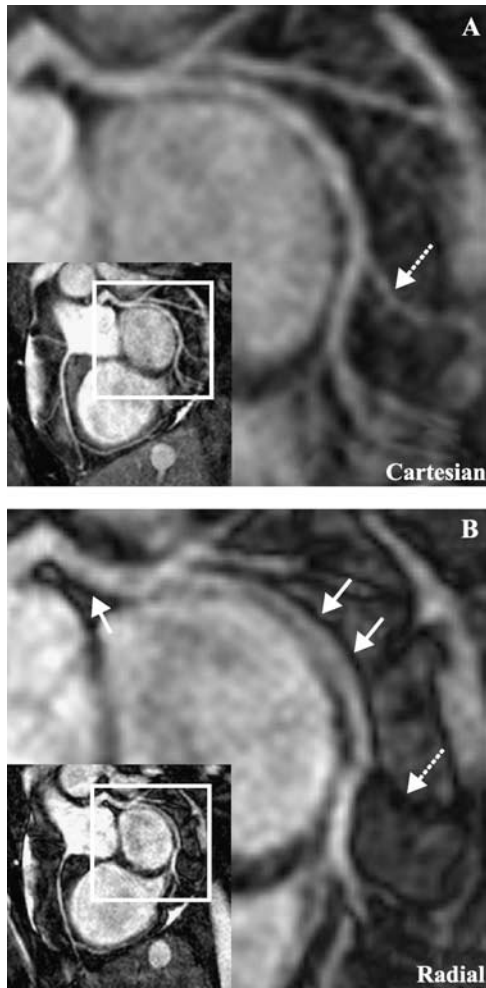
Figure 1. Multiplanar reformatted MR images of the right coronary artery, left main, and the left circumflex artery acquired with Cartesian (A) and radial (B) data acquisition. Please note the markedly improved visualization of coronary side branches with the Cartesian approach. The zoomed display window demonstrates the dark edge artifact (B, solid arrows) with radial imaging; the decreased visualization of side branches with radial SSFP can be explained by two fused black edge artifacts without a remaining visible vessel lumen (dotted arrows).

Magnetic Resonance Imaging

All patients were examined in the supine position using a 1.5 T whole body MR system (Philips Intera CV, Best, The Netherlands) equipped with a Power-Trak6000 gradient system (23 mT/m; 219 μsec rise time) and specifically designed software (Release 9). A five-element cardiac synergy coil was used for signal reception. Cardiac synchronization was performed using four electrodes placed on the left anterior

hemithorax (vector-ECG) and scans were triggered on the R-wave of the ECG (Fischer et al., 1999). A rapid gradient echo sequence (multistack, multislice survey, SSFP, TR/TE/flip angle: 4.0 ms/1.3 ms/55°) allowed for localization of the heart in the three standard planes (transverse, sagittal and coronal). Subsequently, a fast navigator-gated and -corrected (Stuber et al., 1999b) transverse low resolution 3D SSFP scan (TR/TE/flip angle: 3.4 ms/1.3 ms/70°) was performed in the target region with the navigator positioned on the dome of the right hemidiaphragm (5 mm gating window). Using a scan with a transversal slice orientation (cine-SSFP, retrospective gating, 40 phases/cardiac cycle), the rest periods of the left and right coronary artery were individually determined after placing a region of interest on the cross section of the respective coronary artery. The rest period was defined as the duration of the coronary artery moving less than 25% of its cross-sectional area. Thereafter, coronary MRA of the left ($n=20$) or right ($n=24$) coronary artery was performed twice. Magnetic resonance data were acquired once with Cartesian and again with radial k-space filling (random order). Cartesian data acquisition was performed using a centric-ordered (low–high) k-space acquisition scheme. Radial data acquisition was performed using continuous radial sampling in the k_x–k_y-plane, whereas k_z was acquired using conventional Fourier phase encoding. The number of projections was equal to the number of radial sample points ($n=352$) using an undersampling of 0.6. All other parameters (spatial resolution, TR, TE, flip angle, prepulses) were identical to the Cartesian scan.

Twenty overcontiguous slices were obtained using a flow-independent steady-state free precession sequence (TR/TE/flip angle: 4.5 ms/2.3 ms/90°) employing a fat suppression and a T2 preparation prepulse (Botnar et al., 1999b; Brittain et al., 1995). In-plane spatial resolution was 1.0×1.0 mm with a 3-mm-slice thickness. The acquisition duration per heartbeat was adapted with regard to the individual rest period of the respective coronary artery with a predefined maximum of 90 ms. The three-point planscan tool was used for

Table 2. Type and occurence of imaging artifacts caused by the radial k-space sampling technique.

Type	Occurence radial % (no.)	Occurence Cartesian % (no.)
Opposed-phase artifact	91 (40/44)	0 (0/44)
Radial streaks	73 (32/44)	0 (0/44)

planning the optimal imaging plane of the coronary scan (Stuber et al., 1999b): for the left coronary system, the first reference point was the origin of the left main artery, the second a distal point of the LAD, and the third reference point was chosen in the mid- to distal LCX segment. For the right coronary system, three reference points along the main axis of the vessel were indicated. Correction of breathing motion was done with a real-time prospective navigator. Navigator efficiency was defined as the number of accepted navigator gated acquisitions divided by the total number of navigator acquisitions (values are given in %).

Image Analysis

Due to the use of radial as a new approach for coronary MRA, the occurrence and type of radial-related imaging artifacts were noted by two readers in order to assess image quality (Glover and Pauly, 1992). Six months later, repeat analysis of the imaging artifacts was carried out by one of the readers with the scans presented in a random order. For visual evaluation the following 16 segments of the coronary arteries were classified with reference to the suggested ACC/AHA guidelines (Scanlon et al., 1999): 1) left
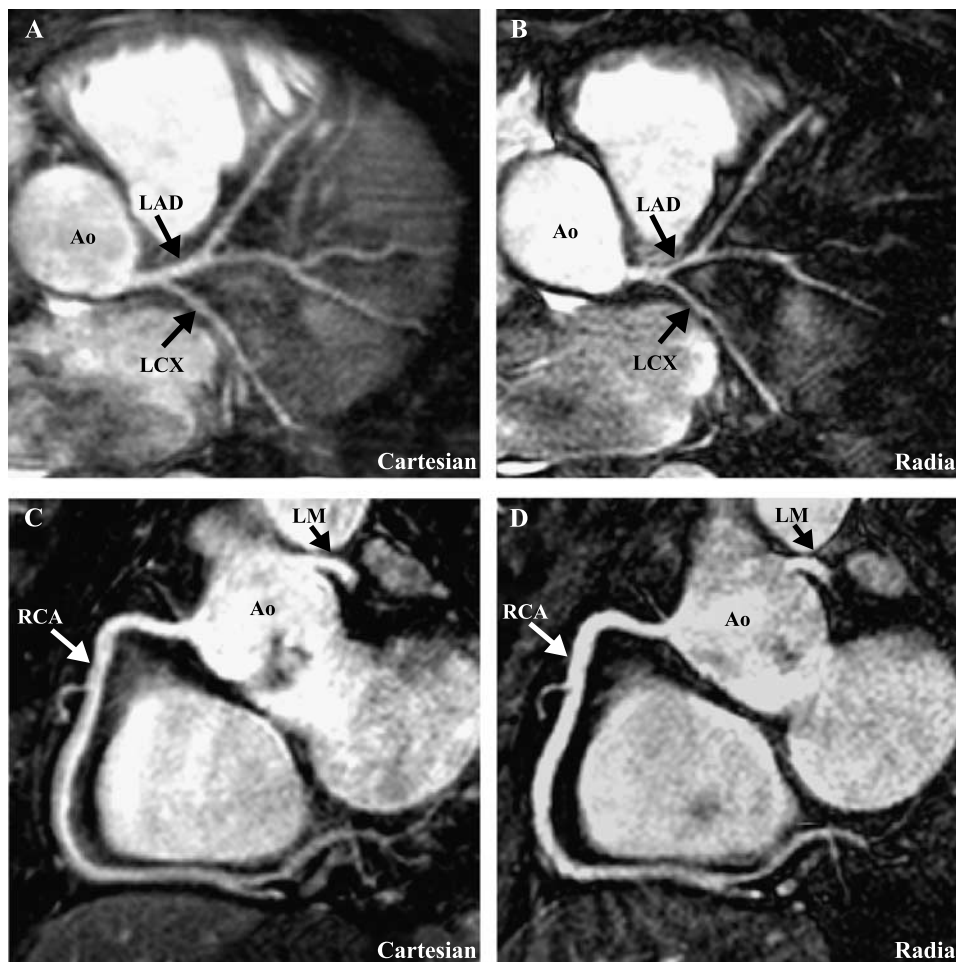
Figure 2. (A, B) Multiplanar reformatted MR images acquired with Cartesian and radial data acquisition of the left coronary artery system. Please note the improved vessel border delineation of the left coronary artery system in radial imaging. For Cartesian data acquisition the increased visibility of the LCX and the coronary side branches particularly with regard to the distal segments can be appreciated. (C, D) Multiplanar reformatted MR images of the right coronary artery acquired with Cartesian and radial data acquisition. Note the increased vessel sharpness with the radial approach and the improved image quality of the visible side branches of the RCA with the Cartesian approach. *Abbreviations*: LAD=left anterior descending artery; LCX=left circumflex artery; Ao=aorta; RCA=right coronary artery; LM=left main.

main segment, 2) proximal segment of LAD, 3) mid-segment of LAD, 4) distal segment of LAD, 5) first diagonal branch, 6) second diagonal branch, 7) proximal segment of LCX, 8) mid segment of LCX, 9) distal segment of LCX, 10) first marginal branch, 11) second marginal branch, 12) proximal segment of RCA, 13) mid segment of RCA, 14) distal segment of RCA, 15) right posterolateralis segment (RPL), and 16) posterolateral descending artery segment (PDA).

A visual score was used to grade the visibility of the coronary vessel segments: 1, poor/uninterpretable (coronary artery visible with markedly blurred borders); 2, good (coronary artery visible with moderately blurred borders); 3, very good (coronary artery visible with mildly blurred borders); 4, excellent (coronary artery visible with sharply defined borders) (Kim et al., 2001).

For the assessment of interobserver and intraobserver variability, two readers independently assessed the visual score, and after a six-month period one of the readers reevaluated the randomly ordered scans. For objective assessment of vessel sharpness, a previously published dedicated quantitative coronary analysis tool with an edge detection and vessel sharpness algorithm was applied on the raw data (Etienne et al., 2002a,b). Vessel sharpness was defined as the average signal along the vessel border on the edge image with higher values identifying better vessel delineation (Botnar et al., 1999b). The values were determined for the first 4 cm of the proximal segments of the LAD, LCX, and RCA. For quantification of angiographic parameters and visualization of coronary artery anatomy, multiplanar reformatting of the 3D data set was carried out with the
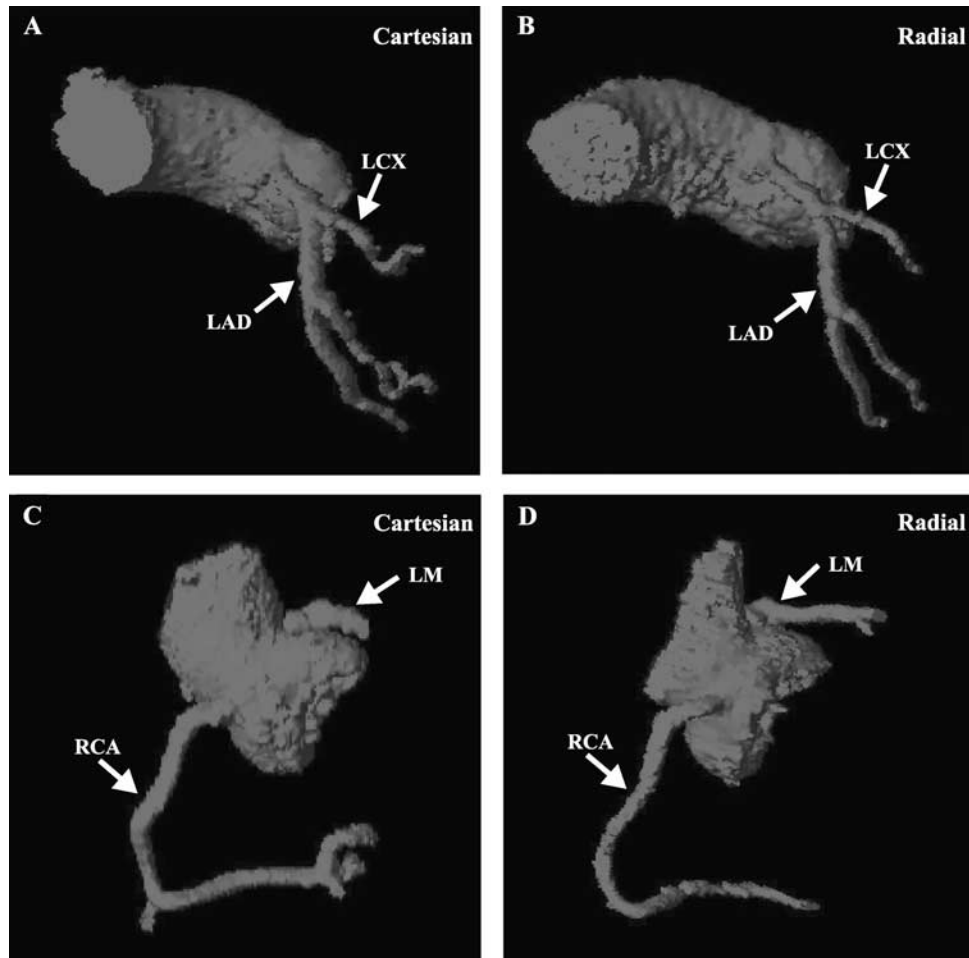
Figure 3. Three dimensional-volume rendering of the left (A, B) and right (C, D) coronary artery with Cartesian and radial approach. Note the improved vessel sharpness, the smaller vessel diameter, and the poorer visibility of coronary side branches with the radial technique. Additionally, the decreased visible vessel length of the left circumflex artery is demonstrated. *Abbreviations*: LAD=left anterior descending artery; LCX=left circumflex artery; RCA=right coronary artery; LM=left main.

Table 3. Comparison of Cartesian and radial data acquisition regarding quantitative MR angiographic parameters.

		Cartesian	Radial	p
LAD	Branches	3.2±1.5	2.3±0.9	0.009
	Length (mm)	91.2±19.7	83.7±25.3	0.065
	Diameter (mm)	3.0±0.5	2.5±0.3	<0.001
	Sharpness (%)	46.0±6.2	56.3±5.7	<0.001
LCX	Branches	2.1±1.4	1.6±0.9	0.008
	Length (mm)	71.6±20.1	58.3±26.1	0.036
	Diameter (mm)	2.8±0.3	2.4±0.7	0.008
	Sharpness (%)	43.6±7.4	49.8±5.4	0.002
RCA	Branches	3.5±1.9	2.3±1.3	<0.001
	Length (mm)	127.1±26.5	123.0±21.9	0.27
	Diameter (mm)	3.2±0.4	2.8±0.5	<0.001
	Sharpness (%)	47.4±7.3	58.9±7.2	<0.001

same software facilitating the measurement of vessel length, average luminal diameter (measured within the first 4 cm from the origin of LAD, LCX, and RCA), and assessment of the number of visible side branches.

The following classification was used for visual assessment of stenosis detection: significant stenosis ($\geq$50% diameter reduction) or occlusion, absence of significant stenosis, or impossible to evaluate. A segmental reduction or signal loss in the MR image was considered to be indicative of a significant coronary artery stenosis or occlusion (Kim et al., 2001; Manning et al., 1993b; Pennell et al., 1993).

Invasive Coronary Angiography

All patients underwent coronary X-ray angiography within three weeks after MR imaging. The conventional coronary angiography was performed using the transfemoral Judkins approach with a selective catheterization of the left and right coronary artery system in multiple projections. An experienced interventionalist blinded to the results of the MR examinations visually evaluated the angiograms. A diameter reduction of $\geq$50% was considered a relevant stenosis.

Statistical Analysis

Statistical analysis was performed using the SPSS software package release 11.01. For all continuous parameters, mean±standard deviation are given. Analysis for statistical differences between the two MR imaging techniques was performed as follows: group differences were tested for continuous variables using the paired Student's T-Test and for categorical variables using the Wilcoxon test. A contingency analysis with Chi-square test or Fisher's exact test was used to calculate sensitivity, specificity, and diagnostic accuracy; to assess statistical significance analysis of variance (ANOVA) was used. Cohen's kappa was applied to measure agreement between the two readings of the first reader (intraobserver variability) and between the two different readers (interobserver variability) using the following grading: 0 to 0.2 (poor), 0.21 to 0.4 (fair), 0.41 to 0.6 (moderate), 0.61 to 0.8 (substantial), 0.81 to 1.0 (nearly perfect). All tests were two-tailed; p<0.05 was considered statistically significant.

RESULTS

Scan Duration and Navigator Efficiency

Nominal scan duration was 217±52 s for the Cartesian and 278±64 s for the radial approach (p<0.01). Depending on the navigator efficiencies, the effective scan duration showed a wide range of variability (Cartesian: 2 min 58 s to 20 min 59 s; radial: 4 min 16 s to 19 min 39 s) (Table 1).

Table 4. Comparison of Cartesian and radial data acquisition for evaluation of coronary artery stenoses.

	Evaluation possible % (no.)	Sensitivity % (no.)	Specificity % (no.)	Accuracy % (no.)
Cartesian	72.9 (248/340)	79.1 (34/43)	84.9 (174/205)	83.9 (208/248)
Radial	65.9 (224/340)*	79.5 (31/39)	81.1 (150/185)	80.8 (181/224)

*p<0.05.

Radial-Related Imaging Artifacts

The following relevant imaging artifacts were found with respect to the radial sampling scheme: radial streak artifacts accentuated in the MR imaging periphery; opposed-phase artifacts along the anatomic water-fat boundaries (example in Fig. 1, data in Table 2). For the two types of artifacts, the inter- and intraobserver agreement was perfect ($\kappa=1.0$ for both, respectively).

Magnetic Resonance Angiographic Parameters

The visual score of the initial read for Cartesian vs. radial data acquisition was 2.9 ± 0.8 vs. 2.7 ± 0.7 ($p=0.09$) for the LAD, 3.0 ± 1.0 vs. 2.2 ± 1.0 for the LCX ($p=0.01$),

and 3.1 ± 1.0 vs. 2.8 ± 0.9 ($p=0.08$) for the RCA. For both MR techniques, interobserver (Cartesian: $\kappa=0.84$; radial: $\kappa=0.87$) and intraobserver agreement (Cartesian: $\kappa=0.86$; radial: $\kappa=0.87$) was nearly perfect.

The following results could be demonstrated for all three coronary arteries (LAD, LCX, and RCA): with the radial approach a significant increase in vessel sharpness was found; while the number of visible side branches and the maximal luminal diameter decreased significantly (examples in Figs. 2 and 3; data in Table 3).

The visible vessel length of LAD and RCA showed no significant differences between both techniques; on the other hand, the LCX demonstrated a significantly decreased visible vessel length with radial data acquisition.
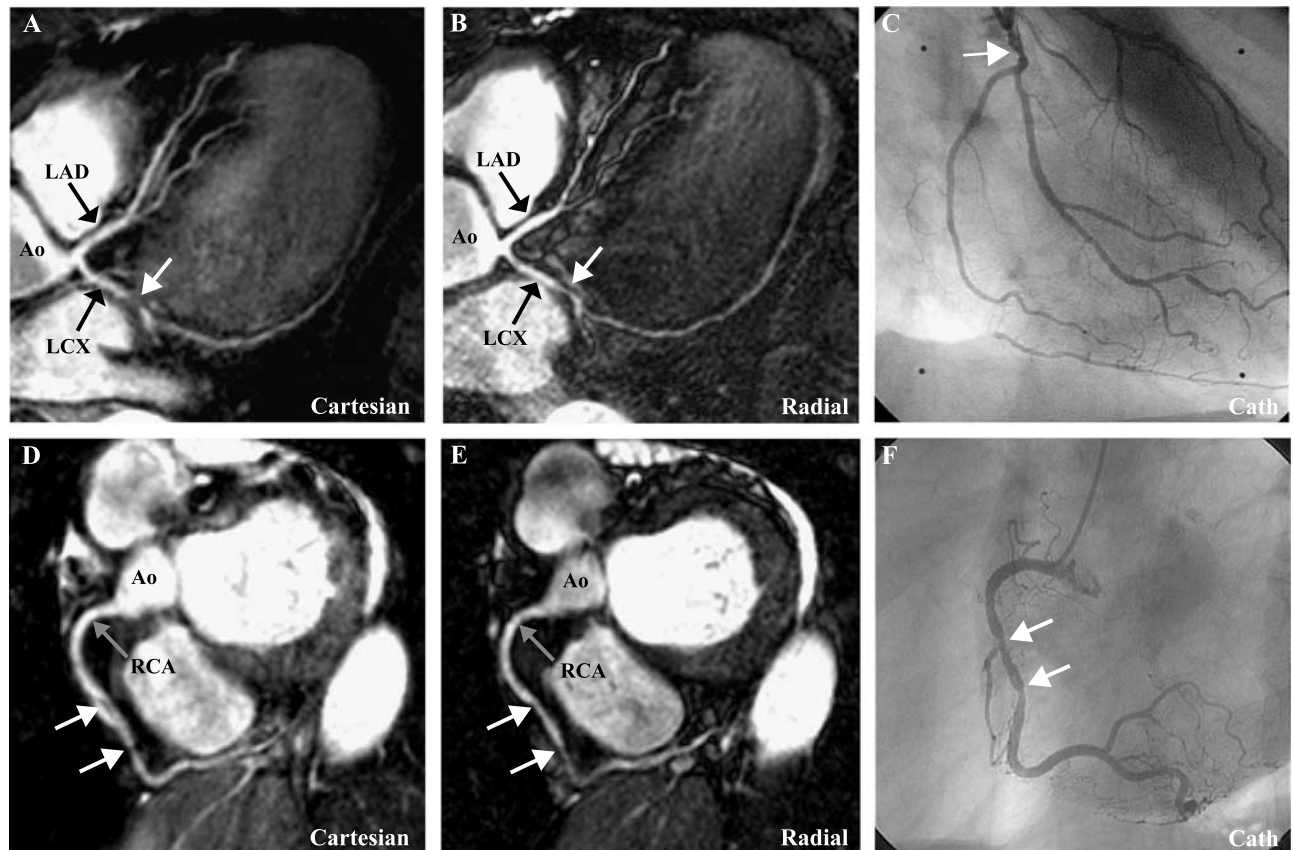
Figure 4. For both Cartesian (A) and radial coronary MRA (B), a significant stenosis of the proximal LCX is demonstrated (white arrow). Conventional coronary angiogram (C) confirmed a 75% stenosis of the LCX (white arrow). Note that the ''soap-bubble visualization'' of the 3D coronary MRA data set displays the findings of biplane conventional coronary angiography in one imaging plane. Conventional coronary angiogram (F) demonstrating a 60% stenosis of the mid-RCA and a 50% stenosis of the distal RCA (white arrows). Both Cartesian (D) and radial coronary MRA (E) show the right coronary artery containing the two stenoses (white arrows) in the identical location in the same patient. *Abbreviations*: LAD=left anterior descending artery; LCX=left circumflex artery; Ao=aorta; RCA=right coronary artery.

Invasive Coronary Angiography

In conventional X-ray angiography, 32 of 44 patients (73%) had significant coronary artery disease: 8 patients had one-vessel disease, 7 had two-vessel disease, and 17 patients had three-vessel disease. All evaluated coronary artery segments showed maximal one stenotic lesion.

Diagnostic Accuracy of Coronary MRA

With radial data acquisition, 116 of 340 coronary artery segments (34%) had to be excluded from further analysis due to poor image quality (Table 4). Of the remaining 224 segments, 31 of 39 significant coronary artery stenoses/occlusions as well as the absence of significant stenoses in 150 of 185 segments were correctly identified. Sensitivity, specificity and diagnostic accuracy are listed in Table 4.

With the Cartesian approach 92 of 340 coronary artery segments (27%) could not be evaluated due to poor image quality. Of the 248 evaluable segments, 34 of 43 significant coronary artery stenoses/occlusions and the absence of significant stenoses in 174 of 205 segments were correctly identified (Table 4, examples shown in Fig. 4).

DISCUSSION

The present study directly compared radial and Cartesian k-space data acquisition for coronary MRA using steady-state free precession sequences. We found a significant increase in vessel sharpness for the radial approach, whereas the total number of visible side branches, the visible vessel length of the left circumflex artery, and, consequently, the total number of assessable coronary artery segments were significantly decreased. Both techniques yielded comparable results regarding the visual score and the visible vessel length for the LAD and RCA territory. Diagnostic performance was similar for both techniques as well.

Optimally, coronary MRA should image the whole coronary arterial tree including distal segments and side branches and should allow reliable detection of coronary artery stenosis. The radial k-space acquisition technique seemed to be a promising approach for improved coronary artery imaging during navigator-gated free-breathing coronary MRA, offering several advantages over Cartesian Fourier techniques. Radial acquisition techniques are particularly insensitive to motion due to signal averaging of low spatial fre-

quencies from oversampling of central k-space data. Additional benefits result from portrayal of artifacts as radial streaks, with the amplitude being smallest near to the moving elements as well as streak deployment perpendicular to the direction of object motion, often residing outside the anatomic boundaries of the subject (Glover and Pauly, 1992). Thus, the occurrence of peripheral radial streak artifacts did not influence coronary depiction. In order to satisfy Nyquist's sampling theorem in radial scans, the total number of projections required is given by: $(\pi/2) \times (number\ of\ radial\ sample\ points)$. Undersampling in the angular direction results also in streaking artifacts. For the present study, an undersampling of 0.6 was used, which has been reported to result in no severe loss of image quality (Rasche et al., 1994).

Up to now, there are only a few studies dealing with the application of radial k-space data acquisition. Phantom and in vivo experiments demonstrated the feasibility of using the radial sequence for real-time cardiac cine imaging (Larson and Simonetti, 2001; Spuentrup et al., 2003c). The present study demonstrates that the use of radial k-space data acquisition for coronary MRA is feasible as well. Primarily, the radial approach benefits from the distinct increase in vessel sharpness. On the other hand, significantly less coronary side branches were visualized, representing a definite drawback. Both effects are mainly related to the occurrence of dark edge artifacts: these can be explained by the opposed-phase phenomenon resulting from continuously decreasing fat suppression during the data acquisition window per heartbeat, despite limiting the acquisition duration to a maximum of 90 ms. Consequently, with the radial technique, the coronary side branches with their smaller luminal diameter occurred as two fused black lines without a remaining visible vessel lumen (example in Fig. 1). This effect applies to the distal left circumflex artery as well, resulting in a shorter visible vessel length of the LCX with radial imaging. On the other hand, proximal and mid-coronary artery segments with a larger luminal diameter demonstrated an extremely improved vessel border definition due to the dark edge. At the same time, this edge artifact, yielded a decreased vessel diameter and may eventually lead to misinterpretation as stenotic narrowing, although the comparison to the Cartesian approach showed no differences with regard to the diagnostic accuracy. The decreasing effectiveness of the fat suppression prepulse during readout of the image information plays a pivotal role for the radial approach only: all k-lines being sampled influence image contrast, while the low-high centric ordered k-space acquisition with the Cartesian approach always ensures a sufficient

fat suppression during data readout of the contrast-relevant k-lines. This marked edge artifact is the common cause for decreased visualization of side branches, smaller luminal vessel diameter, and increased vessel sharpness using the radial technique. To prevent the occurrence of this artifact, further limitations to the acquisition duration per heartbeat may be required; however, this will equivalently increase the total scan duration. However, with radial SSFP the total scan duration is already significantly longer using an acquisition duration of maximal 90 ms.

In addition some off-resonance effects were associated with radial sampling. One of them is the broadening of the point-spread-function (PSF), with the effect of blurring structures in image space (Rasche et al., 1999). Moreover, there is an increase in blood signal oscillations for SSFP-sequences with an increase in off-resonance frequency, which will lead to increased image artifacts (Deshpande et al., 2001). Reeder et al. (1998) have reported that resonance offsets on the order of 100 Hz may exist in the heart in the vicinity of the cardiac veins (i.e., LCX, first diagonal branch). A change of the volume acquisition scheme may overcome this disadvantage (Stehning et al., 2003). All mentioned effects were relevant to the radial but not to the Cartesian technique.

However, it is noteworthy that all findings of the present study were valid for the examination of consecutive patients: the radial acquisition scheme may improve coronary MR imaging in patients with cardiac arrhythmias since it is less sensitive to motion artifacts (Spuentrup et al., 2003b). Further studies are needed to verify this assumption.

CONCLUSIONS

The SSFP with radial k-space sampling proved to be a feasible approach for coronary artery imaging in a consecutive patient population. Coronary MRA with radial k-space sampling appears to be on a par with the Cartesian approach with respect to the diagnostic accuracy of stenosis detection. Nevertheless, with current implementations radial k-space data acquisition is inferior to the Cartesian acquisition scheme regarding the visualization of side branches despite better vessel sharpness.

ACKNOWLEDGMENTS

REFERENCES

Bornert, P., Jensen, D. (1995). Coronary artery imaging at 0.5 T using segmented 3D echo planar imaging. *Magn. Reson. Med.* 34(6):779–785.

Bornert, P., Aldefeld, B., Nehrke, K. (2001). Improved 3D spiral imaging for coronary MR angiography. *Magn. Reson. Med.* 45(1):172–175.

Botnar, R. M., Stuber, M., Danias, P. G., Kissinger, K. V., Manning, W. J. (1999a). A fast 3D approach for coronary MRA. *J. Magn. Reson. Imaging* 10(5):821–825.

Botnar, R. M., Stuber, M., Danias, P. G., Kissinger, K. V., Manning, W. J. (1999b). Improved coronary artery definition with T2-weighted, free-breathing, three-dimensional coronary MRA. *Circulation* 99(24):3139–3148.

Brittain, J. H., Hu, B. S., Wright, G. A., Meyer, C. H., Macovski A., Nishimura, D. G. (1995). Coronary angiography with magnetization-prepared T2 contrast. *Magn. Reson. Med.* 33(5):689–696.

Danias, P. G., McConnell, M. V., Khasgiwala, V. C., Chuang, M. L., Edelman, R. R., Manning, W. J. (1997). Prospective navigator correction of image position for coronary MR angiography. *Radiology* 203(3):733–736.

Deshpande, V. S., Shea, S. M., Laub, G., Simonetti, O. P., Finn, J. P., Li, D. (2001). 3D magnetization-prepared true-FISP: a new technique for imaging coronary arteries. *Magn. Reson. Med.* 46(3):494–502.

Duerk, J. L., Lewin, J. S., Wendt, M., Petersilge, C. (1998). Remember true FISP? A high SNR, near 1-second imaging method for T2-like contrast in interventional MRI at .2 T. *J. Magn. Reson. Imaging* 8(1):203–208.

Etienne, A., Boesiger, P., Manning, W., Nagel, E., Botnar, R., Stuber, M. (2002a). Quantitative coronary analysis and visualization based on three dimensional coronary magnetic resonance angiography. *J. Cardiovasc. Magn. Reson.* 4:90.

Etienne, A., Botnar, R. M., Van Muiswinkel, A. M., Boesiger, P., Manning, W. J., Stuber, M. (2002b). ''Soap-Bubble'' visualization and quantitative analysis of 3D coronary magnetic resonance angiograms. *Magn. Reson. Med.* 48(4):658–666.

Fischer, S. E., Wickline, S. A., Lorenz, C. H. (1999). Novel real-time R-wave detection algorithm based on the vectorcardiogram for accurate gated

magnetic resonance acquisitions. *Magn. Reson. Med.* 42(2):361–370.

Glover, G. H., Pauly, J. M. (1992). Projection reconstruction techniques for reduction of motion effects in MRI. *Magn. Reson. Med.* 28(2):275–289.

Kim, W. Y., Danias, P. G., Stuber, M., Flamm, S. D., Plein, S., Nagel, E., Langerak, S. E., Weber, O. M., Pedersen, E. M., Schmidt, M., Botnar, R. M., Manning, W. J. (2001). Coronary magnetic resonance angiography for the detection of coronary stenoses. *N. Engl. J. Med.* 345(26):1863–1869.

Larson, A. C., Simonetti, O. P. (2001). Real-time cardiac cine imaging with SPIDER: steady-state projection imaging with dynamic echo-train readout. *Magn. Reson. Med.* 46(6):1059–1066.

Li, D., Kaushikkar, S., Haacke, E. M., Woodard, P. K., Dhawale, P. J., Kroeker, R. M., Laub, G., Kuginuki, Y., Gutierrez, F. R. (1996). Coronary arteries: three-dimensional MR imaging with retrospective respiratory gating. *Radiology* 201(3):857–863.

Li, D., Carr, J. C., Shea, S. M., Zheng, J., Deshpande, V. S., Wielopolski, P. A., Finn, J. P. (2001). Coronary arteries: magnetization-prepared contrast-enhanced three-dimensional volume-targeted breath-hold MR angiography. *Radiology* 219(1): 270–277.

Manning, W. J., Li, W., Boyle, N. G., Edelman, R. R. (1993a). Fat-suppressed breath-hold magnetic resonance coronary angiography. *Circulation* 87(1):94–104.

Manning, W. J., Li, W., Edelman, R. R. (1993b). A preliminary report comparing magnetic resonance coronary angiography with conventional angiography. *N. Engl. J. Med.* 328(12):828–832.

Pennell, D. J., Keegan, J., Firmin, D. N., Gatehouse, P. D., Underwood, S. R., Longmore, D. B. (1993). Magnetic resonance imaging of coronary arteries: technique and preliminary results. *Br. Heart J.* 70(4):315–326.

Rasche, V., Holz, D., Schepper, W. (1994). Radial turbo spin echo imaging. *Magn. Reson. Med.* 32(5): 629–638.

Rasche, V., Holz, D., Proksa, R. (1999). MR fluoroscopy using projection reconstruction multi-gradient-echo (prMGE) MRI. *Magn. Reson. Med.* 42(2):324–334.

Reeder, S. B., Faranesh, A. Z., Boxerman, J. L., McVeigh, E. R. (1998). In vivo measurement of T*2 and field inhomogeneity maps in the human heart at 1.5 T. *Magn. Reson. Med.* 39(6):988–998.

Regenfus, M., Ropers, D., Achenbach, S., Schlundt, C., Kessler, W., Laub, G., Moshage, W., Daniel, W. G. (2003). Diagnostic value of maximum intensity projections versus source images for assessment of contrast-enhanced three-dimensional breath-hold magnetic resonance coronary angiography. *Invest. Radiol.* 38(4):200–206.

Scanlon, P. J., Faxon, D. P., Audet, A. M., Carabello, B., Dehmer, G. J., Eagle, K. A., Legako, R. D., Leon, D. F., Murray, J. A., Nissen, S. E., Pepine, C. J., Watson, R. M., Ritchie, J. L., Gibbons, R. J., Cheitlin, M. D., Gardner, T. J., Garson, A. Jr., Russell, R. O. Jr., Ryan, T. J., Smith, S. C. Jr. (1999). ACC/AHA guidelines for coronary angiography. A report of the American College of Cardiology/American Heart Association Task Force on practice guidelines (Committee on Coronary Angiography). Developed in collaboration with the Society for Cardiac Angiography and Interventions. *J. Am. Coll. Cardiol.* 33(6):1756–1824.

Shea, S. M., Deshpande, V. S., Chung, Y. C., Li, D. (2002). Three-dimensional true-FISP imaging of the coronary arteries: improved contrast with T2-preparation. *J. Magn. Reson. Imaging* 15(5):597–602.

Spuentrup, E., Bornert, P., Botnar, R. M., Groen, J. P., Manning, W. J., Stuber, M., (2002). Navigator-gated free-breathing three-dimensional balanced fast field echo (TrueFISP) coronary magnetic resonance angiography. *Invest. Radiol.* 37(11):637–642.

Spuentrup, E., Buecker, A., Stuber, M., Botnar, R., Nguyen, T. H., Bornert, P., Kolker, C., Gunther, R. W. (2003a). Navigator-gated coronary magnetic resonance angiography using steady-state-free-precession: comparison to standard t2-prepared gradient-echo and spiral imaging. *Invest. Radiol.* 38(5):263–268.

Spuentrup, E., Buecker, A., Stuber, M., Kuhl, H. P. (2003b). Images in cardiovascular medicine. Visualization of anomalous coronary artery in the presence of arrhythmia using radial balanced fast field echo coronary magnetic resonance angiography. *Circulation* 107(23):e214.

Spuentrup, E., Schroeder, J., Mahnken, A. H., Schaeffter, T., Botnar, R. M., Kuhl, H. P., Hanrath, P., Gunther, R. W., Buecker, A. (2003c). Quantitative assessment of left ventricular function with interactive real-time spiral and radial MR imaging. *Radiology* 227(3):870–876.

Stehning, C., Börnert, P., Nehrke, K., Schäffter, T., Dössel, O. (2003). Radial balanced FFE imaging with extended sampling windows for fast coronary MRA. *Proc. ISMRM (abstract)* 11:732.

Stuber, M., Botnar, R. M., Danias, P. G., Kissinger, K. V., Manning, W. J. (1999a). Submillimeter three-dimensional coronary MR angiography with real-time navigator correction: comparison of navigator locations. *Radiology* 212(2):579–587.

Stuber, M., Botnar, R. M., Danias, P. G., Sodickson, D. K., Kissinger, K. V., Van Cauteren, M., De Becker, J., Manning, W. J. (1999b). Double-oblique free-breathing high resolution three-dimensional coronary magnetic resonance angiography. *J. Am. Coll. Cardiol.* 34(2):524–531.

Thedens, D. R., Irarrazaval, P., Sachs, T. S., Meyer, C. H., Nishimura, D. G. (1999). Fast magnetic resonance coronary angiography with a three-dimensional stack of spirals trajectory. *Magn. Reson. Med.* 41(6):1170–1179.

Yang, P. C., Meyer, C. H., Terashima, M., Kaji, S., McConnell, M. V., Macovski, A., Pauly, J. M., Nishimura, D. G., Hu, B. S. (2003). Spiral magnetic resonance coronary angiography with rapid real-time localization. *J. Am. Coll. Cardiol.* 41(7):1134–1141.